A Simplified Predictive Torque Control Scheme for Open-End Winding Induction Motor Drive

Kodumur Meesala Ravi Eswar, Kunisetti Venkata Praveen Kumar, and Thippiripati Vinay Kumar, *Member, IEEE*

***Abstract*— Variable speed induction motor (IM) drives with predictive torque control (PTC) technique is an advancing technology nowadays. The PTC technique is introduced for dual-inverter fed open-end winding IM (OEWIM) configuration owing to its benefits. The conventional PTC requires flux weighting factor assignment because of two different control objectives (torque and flux) in single cost function. This weighting factor selection plays a key role in selecting optimal voltage vector for better torque and flux response. Several analytical and empirical methods are introduced for optimal selection of weighting factor, which demands more computation time. This paper aims to develop modified PTC, eliminating flux weighting factor. The flux control objective is replaced by an equivalent reactive torque control. Thus making two control objectives of the same units and eliminating the requirement of flux weighting factor in cost function. Furthermore, nearest voltage vector selection strategy is introduced to limit the number of prediction voltage vectors in each sampling period. Thus, overall computational burden is reduced achieving minimum torque and flux ripples. The performance of the proposed PTC for multilevel inversion fed OEWIM is evaluated through MATLAB/Simulink simulations and experimental analysis. To highlight its benefits, these results are compared with those of the conventional and recent PTC techniques.**

***Index Terms*— Dual-inverter fed open-end winding induction motor (OEWIM), nearest voltage vector selection, predictive torque control (PTC), reactive torque control, weighting factor elimination.**

I. Introduction

THE application of voltage source inverter (VSI) in variable speed motor drives became more popular. The present research establishes that the precise control of motor drive is possible, as the number of voltage vectors increases while using the multilevel VSIs (MLI) in electric drive applications [1]. Various MLI configurations are documented in [2]–[4]. Apart from these, a dual-inverter fed open-end winding induction motor (OEWIM) configuration facilitates more benefits such as easy availability of two-level VSIs for multilevel inversion, fewer dc link voltages, and the absence of clamping diodes makes the configuration simple compared to cascade H-bridge and neutral point clamped (NPC) structure. In [5], various applications of OEWIM drive are documented. The dynamic performance of a drive can be improved by employing several control methods. In the past 1960s, field-oriented control is the first control technique introduced for electric drive [6], [7], where controlling is in rotating reference frame. The presence of current proportional–integral (PI) regulators, reference frame transformations and rotor flux observer results in complex control structure.

To overcome these limitations, direct torque control (DTC) is introduced [8] for electric drive applications in 1986. It provides controlling in stationary reference frame. It offers simple control structure. However, it has the following drawbacks: the presence of torque and flux hysteresis controllers demands low sampling times in practical implementation, poor torque and flux regulation, and switching frequency dependent on motor speed and hysteresis bands. These limitations are exhibited in [9]–[12]. In [13], DTC technique is introduced for dual-inverter fed OEWIM drive.

Recently, model predictive control (MPC) is introduced in the control process. The MPC scheme is applied for power converter and drive applications [14]. The MPC has two divisions. They are continuous control set MPC and finite control set MPC (FS-MPC). Predictive torque control (PTC) is the part of FS-MPC, becoming popular for electric drive application. The following are the merits of PTC: simple structure, easy control by involving regulation parameters into the cost function, better torque and flux regulation, and intuitive nature. In [15] and [16], PTC is conducted on induction motor (IM) drive with an extended prediction steps. In [17], a five leg ac–dc–ac converter fed IM drive with PTC scheme is implemented. In [18], PTC is achieved on IM drive fed by three-phase four-switch inverter configuration.

The control process involves in PTC is cost function minimization. Several cost function formulations are given in [19]. Basic PTC cost function is the combination of torque and flux control objectives. Since both of these objectives are of different units, to provide relative balance, weighting factor allocation to the respective objective is required. Thus, selection of weighting factor influences the control performance of motor drive. Present research in PTC is to solve the problem of weighting factor selection.

Cortes *et al*. [20] formulated different structures of cost function and weighting factors for motor drive application.

Manuscript received December 3, 2017; revised January 29, 2018 and March 17, 2018; accepted April 20, 2018. Date of publication May 2, 2018; date of current version May 1, 2019. This work was supported in part by the Science and Engineering Research Board-Department of Science and Technology under Grant SERB-DST/EEQ/2016/000188 and in part by the National Institute of Technology, Warangal. Recommended for publication by Associate Editor Luca Zarri. *(Corresponding author: Thippiripati Vinay Kumar.)*

The authors are with the Department of Electrical Engineering, National Institute of Technology, Warangal 506004, India (e-mail: nit.ravieswar@gmail.com; kvpraveenkumar15@gmail.com; tvinay.nitw@gmail.com).

Color versions of one or more of the figures in this paper are available online at http://ieeexplore.ieee.org.

Digital Object Identifier 10.1109/JESTPE.2018.2832240

However, the weighting factor value is considered by empirical procedure for achieving better response. The empirical approach of weighting factor selection is a time consuming process. In [21], genetic algorithm-based approach is followed for weight determination which requires lot of look up process prior to control. In [22], optimal weighting factor is determined for indirect matrix converter fed IM, considering the derivative of torque ripple square with respect to weight is zero. However, this approach is dependent of system parameters and requires more mathematical analysis. In [23], optimal set of weighting factors are determined, performing lot of search process with a broad range of parameter values, which is more complex approach. In [24] and [25], fuzzy technique is introduced in PTC to alleviate weighting factor tuning. However, in [25], the effort of priority coefficient tuning for membership functions cannot be eliminated. In [26], predictive control is performed on matrix converter in the application of volt ampere reactive compensation, where weighting factors are tuned online. However, the autotuning feature demands more computation time. In [27], PTC of IM drive is performed, where the weighting factors are eliminated using multiobjective ranking analysis. However, increase in prediction vectors makes the control process complex as it involves more mathematical analysis. Recently, PTC for OEWIM drive is proposed in [28], where weighting factors in cost function are empirically selected which is cumbersome process. In [29] and [30], multidecision criteria-based technique for order of preference by similarity to ideal solution and VlseKriterijuska Optimizacija I Komoromisno Resenje methods are applied for PTC of IM drive to solve the weighting factor selection problem. However, it demands comprehensive mathematical analysis, thereby increased computational burden of control process. In [31], PTC of OEWIM drive with zero-sequence current suppression is performed considering conventional cost function, where the weighting factors are selected empirically. In [32], an improved PTC technique is introduced for IM drive fed by two-level inverter with limited prediction voltage vectors. In [33] and [34], elimination of weighting factor in PTC of IM drive is performed by introducing new single control objective for combined torque and flux control. In [33], limited prediction voltage vectors are selected by knowing the sector information of stator flux vector and stator flux error. However, the entire scheme involves trigonometric functions which are again additional burden to the processor. In [35], PTC is implemented on OEWIM drive, where the weighting factor is optimized in each sample interval by incorporating self-tuning feature.

In this paper, a dual-inverter fed OEWIM is modeled and its possible effective voltage space vector allocations with unequal dc link voltages of VSIs to achieve four-level inversion are presented. An improved PTC scheme is implemented for the controlling of OEWIM, where the weighing factor in cost function is completely eliminated. A number of prediction voltage vectors are limited based on selection of nearest voltage vectors, thus reducing the computational burden of control process. This feature allows an additional benefit of switching frequency reduction, without including separate switching frequency control objective in cost function. The decrease in dual-inverter switching frequency adds the benefit of common mode voltage (CMV) reduction [36]. The proposed scheme for OEWIM drive is verified through simulation and experimental analysis. Its results are compared with conventional scheme to show the effectiveness of the proposed scheme. This paper structured as follows. Mathematical modeling of dual-inverter fed OEWIM is discussed in Section II. Detailed information about the operation of classical PTC for OEWIM drive is specified in Section III. In Section IV, the proposed PTC and its control concepts are discussed. The validation of the proposed PTC scheme and its effectiveness over classical PTC is illustrated in Section V by performing simulation and experimentation. At long last, conclusions are provided in Section VI.

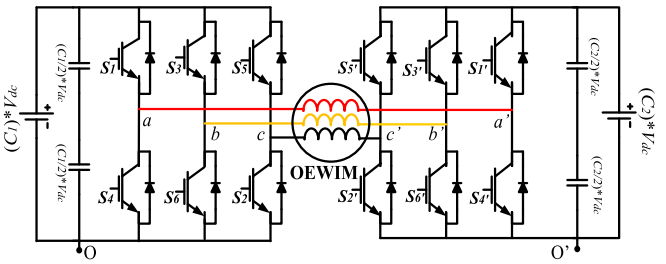

Fig. 1. OEWIM model.

II. Mathematical Equations of Dual-Inverter Fed OEWIM

From Fig. 1, dual-inverter (VSI-1 and VSI-2) pole voltages are represented by (1) and (2). Pole voltages are measured with respect to negative rails of their corresponding VSIs. To obtain four-level inversion, dc link voltages of dual inverter are maintained in 2:1 ratio. Therefore, VSI-1 dc link voltage is set to $C_1 V_{\rm dc}$ where C_1 is 2/3 and VSI-2 dc link voltage is set to $C_2 V_{\rm dc}$ where C_2 is 1/3. S_a, S_b, S_c, S'_a, S'_b, and S'_c are the switching pulses provided to the upper switches (S_1, S_3, S_5, S'_1, S'_3, S'_5) of dual inverter

$$\begin{pmatrix} V_{ao} \\ V_{bo} \\ V_{co} \end{pmatrix} = \begin{pmatrix} S_a \\ S_b \\ S_c \end{pmatrix} * (C_1 V_{\rm dc}) \tag{1}$$

$$\begin{pmatrix} V_{a'o'} \\ V_{b'o'} \\ V_{c'o'} \end{pmatrix} = \begin{pmatrix} S_{a'} \\ S_{b'} \\ S_{c'} \end{pmatrix} * (C_2 V_{\rm dc}). \tag{2}$$

The difference of pole voltages of dual inverter is stated by (3). The sum of pole voltage difference in (4) is not equal to zero is termed as zero-sequence [5] voltage given by (5). Thus by substituting (5) in (4), voltages applied to OEWIM phases are given by (6)

$$\begin{pmatrix} \delta V_{aa'} \\ \delta V_{bb'} \\ \delta V_{cc'} \end{pmatrix} = \begin{pmatrix} V_{ao} - V_{a'o'} \\ V_{bo} - V_{b'o'} \\ V_{co} - V_{c'o'} \end{pmatrix} \tag{3}$$

$$\begin{pmatrix} \delta V_{aa'} \\ \delta V_{bb'} \\ \delta V_{cc'} \end{pmatrix} = \begin{pmatrix} V_{aa'} \\ V_{bb'} \\ V_{cc'} \end{pmatrix} + \begin{pmatrix} V_z \\ V_z \\ V_z \end{pmatrix} \tag{4}$$

$$V_z = \frac{1}{3}(\delta V_{aa'} + \delta V_{bb'} + \delta V_{cc'}) \tag{5}$$

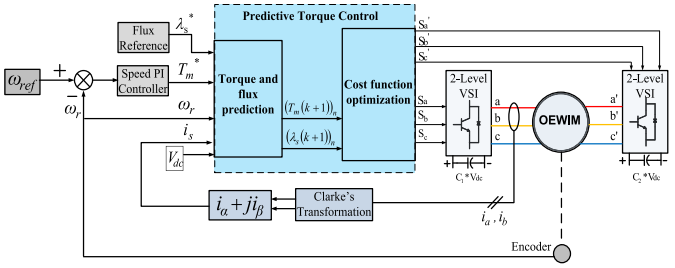

Fig. 2. Classical PTC operational block diagram.

$$\begin{pmatrix} V_{aa'} \\ V_{bb'} \\ V_{cc'} \end{pmatrix} = \begin{pmatrix} 2/3 & -1/3 & -1/3 \\ -1/3 & 2/3 & -1/3 \\ -1/3 & -1/3 & 2/3 \end{pmatrix} * \begin{pmatrix} \delta V_{aa'} \\ \delta V_{bb'} \\ \delta V_{cc'} \end{pmatrix}. \quad (6)$$

The OEWIM is modeled in stationary reference frame. The machine stator and rotor voltage dynamic equations in space vector form are represented by (7) and (8), respectively. Space vector representation of stator and rotor flux linkages is given by (9) and (10), respectively. The subscript-"s" and "r" indicate stator and rotor terms, respectively. The generated electromagnetic motor torque (T_m) and fundamental motor-load torque equation are represented by (11) and (12). Here, the term T_l represents load torque on motor shaft. ω_m and ω_r are motor mechanical and electrical speeds

$$V_s = R_s i_s + p\lambda_s \quad (7)$$

$$0 = R_r i_r + p\lambda_r - j\omega_r \lambda_r \quad (8)$$

$$\lambda_s = L_s i_s + L_m i_r \quad (9)$$

$$\lambda_r = L_m i_s + L_r i_r \quad (10)$$

$$T_m = \frac{3}{2}\frac{P}{2}(\text{imag}(\bar{\lambda}_s * i_s)) \quad (11)$$

$$T_m - T_l = J\frac{d\omega_m}{dt}. \quad (12)$$

The variables, stator current space vector (i_s) and flux space vector (λ_s) are considered as machine state variables. Thus, the state space representation of machine model is stated by the following equations:

$$\frac{di_s}{dt} = R_1\left(R_2\lambda_s - R_3 i_s + K_r(V_s + Ri_s - j\omega_r\lambda_s) + \frac{j\omega_r i_s}{R_1}\right) \quad (13)$$

$$\frac{d\lambda_s}{dt} = (V_s + Ri_s) \quad (14)$$

where $R = -R_s$, $R_1 = (L_m/L_s L_r - L_m^2)$, $R_2 = (R_r/L_m)$, $R_3 = (L_s R_r/L_m)$, $p = (d/dt)$, $K_r = (L_r/L_m)$, $V_s = V_{s\alpha} + jV_{s\beta}$, $i_s = i_{s\alpha} + ji_{s\beta}$, $\lambda_s = \lambda_{s\alpha} + j\lambda_{s\beta}$

P = number of poles in a machine and J is the moment of inertia.

III. Classical PTC

The functional block diagram of classical PTC is represented in Fig. 2. The requirements of classical PTC for its operation are: sensed speed, reference torque, combined dc link voltage, flux reference magnitude, and stator current space vector. Speed PI controller generates torque reference in such a manner to maintain the actual speed of motor nearest to the reference speed. In PTC algorithm, machine model is represented in discrete manner using the mathematical equations (13) and (14) by applying forward Euler's method. Its basic illustration is given as

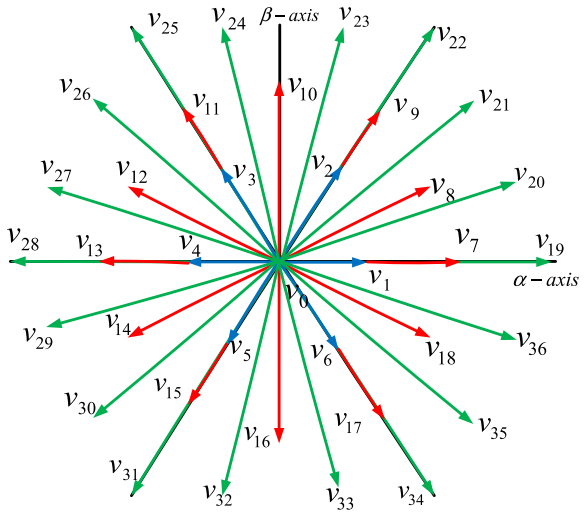

Fig. 3. Dual inverter effective voltage space vector allocations for four-level inversion.

$$\frac{dZ}{dt} = \frac{Z(k+1) - Z(k)}{T_s} \quad (15)$$

where "T_s" is sampling period, "Z" is any state variable, and "k" is present sampling state.

The prime steps involved in classical PTC of OEWIM drive are discussed as follows.

A. Step 1: Measure and Estimate

Dual-Inverter combined dc link voltage and motor speed are directly measured. The machine stator currents (i_a, i_b, and i_c) are directly sensed from the motor phases. The sensed three-phase currents are converted to two phase currents (i_α and i_β) in stationary reference frame using Clarke's transformation. From these, stator current space vector ($i_s = i_\alpha + ji_\beta$) is obtained. Therefore, all the measured quantities (V_{dc}, ω_r, and i_s) are given to PTC algorithm.

In a machine direct measurement of stator flux quantity is not possible. So, stator flux is estimated with the help of Euler's method as stated in (15). Thus, with the knowledge of previous sample state ($k-1$) variables, present sample state (k) stator flux can be estimated as

$$\lambda_s(k) = \lambda_s(k-1) + T_s((V_s(k-1)) + Ri_s(k-1)). \quad (16)$$

B. Step 2: Prediction

The machine stator flux (λ_s) and current (i_s) are predicted for one step ahead ($k+1$) using all the effective voltage space vectors for a given inverter configuration. For dual inverter, with an unequal dc link voltages ($C_1 V_{\text{dc}}$ and $C_2 V_{\text{dc}}$), V_{s1} and V_{s2} are the voltage space vectors generated from VSI-1 and VSI-2, respectively. Their representation is given by (17) and (18). Thus, the effective voltage space vector (V_s) applied

TABLE I
DUAL-INVERTER EFFECTIVE SWITCHING STATES AND VOLTAGE VECTOR REALIZATION IN STATIONARY REFERENCE FRAME

VSI-1	VSI-2	Voltage Space Vector	Realization	
(S_a, S_b, S_c)	(S_a', S_b', S_c')	(V_s)	V_α	V_β
(0,0,0)	(0,0,0)	V_0	0	0
(1,0,0)	(1,0,0)	V_1	$V_{dc}(2/9)$	0
(1,1,0)	(1,1,0)	V_2	$V_{dc}(1/9)$	$(1.7321/9)\ V_{dc}$
(0,1,0)	(0,1,0)	V_3	$V_{dc}(-1/9)$	$(1.7321/9)\ V_{dc}$
(0,1,1)	(0,1,1)	V_4	$V_{dc}(-2/9)$	0
(0,0,1)	(0,0,1)	V_5	$V_{dc}(-1/9)$	$(-1.7321/9)\ V_{dc}$
(1,0,1)	(1,0,1)	V_6	$V_{dc}(1/9)$	$(-1.7321/9)\ V_{dc}$
(1,0,0)	(1,1,1)	V_7	$V_{dc}(4/9)$	0
(1,0,0)	(1,0,1)	V_8	$V_{dc}(1/3)$	$(1.7321/9)\ V_{dc}$
(1,1,0)	(1,1,1)	V_9	$V_{dc}(2/9)$	$(3.4642/9)\ V_{dc}$
(0,1,0)	(0,1,1)	V_{10}	0	$(3.4642/9)\ V_{dc}$
(0,1,0)	(1,1,1)	V_{11}	$V_{dc}(-2/9)$	$(3.4642/9)\ V_{dc}$
(0,1,0)	(1,1,0)	V_{12}	$V_{dc}(-1/3)$	$(1.7321/9)\ V_{dc}$
(0,1,1)	(1,1,1)	V_{13}	$V_{dc}(-4/9)$	0
(0,0,1)	(1,0,1)	V_{14}	$V_{dc}(-1/3)$	$(-1.7321/9)\ V_{dc}$
(0,0,1)	(1,1,1)	V_{15}	$V_{dc}(-2/9)$	$(-3.4642/9)\ V_{dc}$
(0,0,1)	(0,1,1)	V_{16}	0	$(-3.4642/9)\ V_{dc}$
(1,0,1)	(1,1,1)	V_{17}	$V_{dc}(2/9)$	$(-3.4642/9)\ V_{dc}$
(1,0,0)	(1,1,0)	V_{18}	$V_{dc}(1/3)$	$(-1.7321/9)\ V_{dc}$
(1,0,0)	(0,1,1)	V_{19}	$V_{dc}(2/3)$	0
(1,0,0)	(0,0,1)	V_{20}	$V_{dc}(5/9)$	$(1.7321/9)\ V_{dc}$
(1,1,0)	(0,1,1)	V_{21}	$V_{dc}(4/9)$	$(3.4642/9)\ V_{dc}$
(1,1,0)	(0,0,1)	V_{22}	$V_{dc}(1/3)$	$(1.7321/3)\ V_{dc}$
(1,1,0)	(1,0,1)	V_{23}	$V_{dc}(1/9)$	$(1.7321/3)\ V_{dc}$
(0,1,0)	(0,0,1)	V_{24}	$V_{dc}(-1/9)$	$(1.7321/3)\ V_{dc}$
(0,1,0)	(1,0,1)	V_{25}	$V_{dc}(-1/3)$	$(1.7321/3)\ V_{dc}$
(0,1,0)	(1,0,0)	V_{26}	$V_{dc}(-4/9)$	$(3.4642/9)\ V_{dc}$
(0,1,1)	(1,0,1)	V_{27}	$V_{dc}(-5/9)$	$(1.7321/9)\ V_{dc}$
(0,1,1)	(1,0,0)	V_{28}	$V_{dc}(-2/3)$	0
(0,1,1)	(1,1,0)	V_{29}	$V_{dc}(-5/9)$	$(-1.7321/9)\ V_{dc}$
(0,0,1)	(1,0,0)	V_{30}	$V_{dc}(-4/9)$	$(-3.4642/9)\ V_{dc}$
(0,0,1)	(1,1,0)	V_{31}	$V_{dc}(-1/3)$	$(-1.7321/3)\ V_{dc}$
(0,0,1)	(0,1,0)	V_{32}	$V_{dc}(-1/9)$	$(-1.7321/3)\ V_{dc}$
(1,0,1)	(1,1,0)	V_{33}	$V_{dc}(1/9)$	$(-1.7321/3)\ V_{dc}$
(1,0,1)	(0,1,0)	V_{34}	$V_{dc}(1/3)$	$(-1.7321/3)\ V_{dc}$
(1,0,1)	(0,1,1)	V_{35}	$V_{dc}(4/9)$	$(-3.4642/9)\ V_{dc}$
(1,0,0)	(0,1,0)	V_{36}	$V_{dc}(5/9)$	$(-1.7321/9)\ V_{dc}$

to the machine is stated by (19). Out of the possible 64 dual-inverter switching states, the effective switching states are 37 (see Fig. 3). These switching states are categorized into three groups, i.e., small, medium, and large. The voltage vectors $(V_1–V_6)$, $(V_7–V_{18})$, and $(V_{19}–V_{36})$ classified as small, medium, and large, respectively

$$V_{s1} = \left(\frac{2}{3}\right)(C_1 * V_{\rm dc})(S_a + S_b e^{j2\pi/3} + S_c e^{j4\pi/3}) \quad (17)$$

$$V_{s2} = \left(\frac{2}{3}\right)(C_2 * V_{\rm dc})\left(S_a' + S_b' e^{j2\pi/3} + S_c' e^{j4\pi/3}\right) \quad (18)$$

$$V_s = V_{s1} - V_{s2}. \quad (19)$$

Table I represents dual-inverter possible effective switching states and voltage space vectors (V_s) realization in stationary reference frame. Thus, with the information of present sample state variables, stator flux and current are predicted for all the 37 effective voltage vectors as given by (20) and (21). Here,

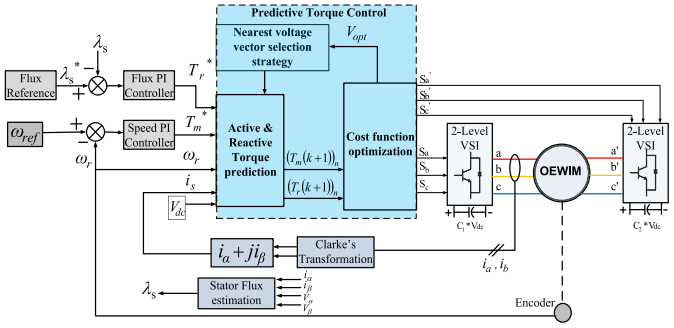

Fig. 4. Proposed PTC operational block diagram.

"n" represents the voltage vector number, i.e., 0 to 36

$$\lambda_s(k+1)_n = \lambda_s(k) + T_s((V_s(k))_n + Ri_s(k)) \quad (20)$$

$$i_s(k+1)_n = i_s(k) + T_s\left(R_1\left(\begin{matrix}R_2\lambda_s(k) - R_3 i_s(k) \\ +K_r((V_s(k))_n + Ri_s(k) \\ -j\omega_r\lambda_s(k)) + \dfrac{j\omega_r i_s(k)}{R_1}\end{matrix}\right)\right). \quad (21)$$

Motor torque prediction at one step ahead for the 37 effective voltage vectors is given as

$$(T_m(k+1))_n = \frac{3}{2}\frac{P}{2}(\text{imag}(\bar{\lambda}_s(k+1)_n * i_s(k+1)_n)). \quad (22)$$

C. Step 3: Cost Function Formulation

In predictive control scheme, the cost function is expressed with different control objectives. These control objectives are organized with control parameter reference and predicted values of the respective control parameter. The cost function formulation plays a key role in PTC, as the control action and realization of optimal switching state in this scheme is performed based on its minimization. The commonly involved control objectives in PTC cost function are motor torque and flux as stated by the following equation:

$$G_n = \left|T_m^* - T_m(k+1)_n\right| + W_f\left|\lambda_s^* - |\lambda_s(k+1)_n|\right|. \quad (23)$$

Here, T_m^* and λ_s^* are the reference values of motor torque and flux, which are compared with their predicted values, respectively. The term "W_f" denotes flux weighting factor, which is assigned to provide the relative importance between torque and flux control objectives. In [28], the value of W_f is considered as the ratio of nominal torque and flux $(T_{\rm nom}/\lambda_{\rm nom})$ of a machine. However, it is only approximated value. Therefore, in real-time operation W_f value need to be adjusted for achieving optimal control response of OEWIM drive.

IV. PROPOSED PTC FOR OEWIM DRIVE

From the classical PTC discussed in Section III, it is observed that the only term need to tune in cost function is flux weighting factor (W_f) and its improper selection leads to distortions in motor torque and flux. Therefore, its proper tuning in order to achieve optimal control response of motor drive becomes one of the major problem. To solve

this problem, various control methods are introduced in the literature. In conventional PTC of OEWIM [28], heuristic procedure is followed for weight determination achieving better torque and flux control response. However, it is a time taking process. Recently in [33], flux weighting factor has completely eliminated by modifying the cost function. New control objective is formulated having the reference and predicted values of stator flux vector. Thus, the combined torque and flux control is possible with a single control objective, thereby eliminating weighting factor. However, the calculation of reference stator flux space vector involves trigonometric functions and parameter dependent.

In this paper, an improved and simple PTC for OEWIM drive is introduced. Fig. 4 depicts functioning block diagram of the proposed PTC.

A. Modified Cost Function Formulation

In a conventional PTC cost function, the difference in control objectives of motor torque and flux, demands weighting factor to provide the relative importance between them. In this paper, a reactive torque control objective is introduced, which is equivalent to the flux control. The modified cost function is stated as

$$G_n = \left|T_m^* - T_m(k+1)_n\right| + \left|T_r^* - T_r(k+1)_n\right|. \quad (24)$$

Here, T_r^* is the reference reactive torque generated from the flux PI controller. The flux in a machine is related to the reactive torque. The basic representation of reactive torque is stated in [37], which is given as

$$T_r = \frac{3}{2}\frac{P}{2}(\text{real}(\bar{\lambda}_s * i_s)). \quad (25)$$

The one step ahead prediction for the reactive torque is given as

$$(T_r(k+1))_n = \frac{3}{2}\frac{P}{2}(\text{real}(\bar{\lambda}_s(k+1)_n * i_s(k+1)_n)). \quad (26)$$

Thus, the closeness of predicted value of reactive torque $[T_r(k+1)]$ with the generated reference reactive torque value (T_r^*) ensures flux control. From (24), it is observed that the first control objective represents electromagnetic torque control and the second control objective represents reactive torque control which is an equivalent flux control, thus ensuring both the control objectives are of the same units. The similarity in control objectives alleviates flux weighting factor assignment in cost function. Thereby, an improved predictive torque and flux control of OEWIM drive is achieved with the modified cost function, eliminating weighting factor.

B. Nearest Voltage Vector Selection

In PTC of OEWIM drive, the optimal voltage vector is the one which gives minimum cost function value. Thus for optimal selection of voltage vector, the modified cost function (24) value needs to be determined for all the 37 dual-inverter voltage states in every sample period. In order to reduce the computational burden of control process, the number of prediction voltage vectors available in each sample interval has to be limited. Recently in [32] and [33], based on the data of sector division and stator flux error, set of limited voltage vectors are made available for the prediction and evaluation of cost function. This requires stator flux vector position information using inverse trigonometric function. However, it demands more computation time and also the number of voltage vectors required for prediction depends on sector information. Hence, it needs more number of voltage vectors when compared to the proposed PTC scheme.

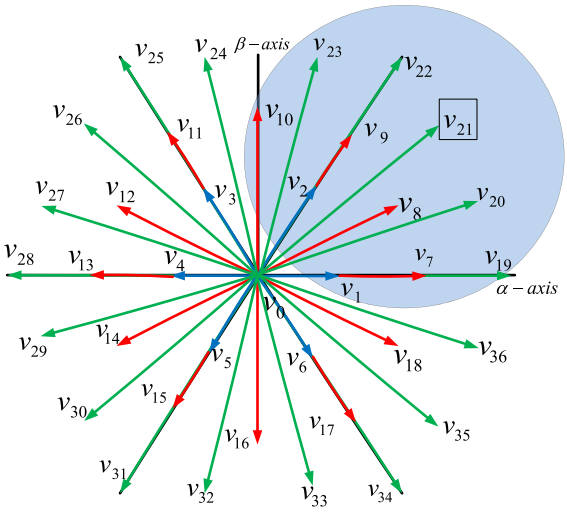

Fig. 5. Possible limited prediction vectors selection for next sample interval when the present optimal vector is V_{21}.

In this paper, prediction voltage vectors are limited by nearest voltage vector selection strategy. It does not require any information about the stator flux vector position and sector. In this, a number of prediction voltage vectors are limited by considering only nearest voltage vectors to the optimal one, which is selected in previous step. With the information of previous optimal voltage vector state, form the nearest voltage vectors set. The set of nearest voltage vectors to the optimal one are determined in such a way that it includes at least one from small vector group, at least four from medium vector group and at least four from large vector group. With this all the group of voltage vector candidates (small, medium, and large) are get involved and thus forming overall 12 limited prediction voltage vectors including null vector. This set of 12 limited prediction voltage vectors are made available for cost function evaluation and from this set, optimal switching state is figured out which gives minimum cost function value (24). Its corresponding switching states are fed to dual inverter switches. This process keeps on continuing.

Considering the case where the voltage vector V_{21} is selected as optimal, now the set of voltage vectors nearer to the optimal vector V_{21} are: V_0, V_1, V_2, V_7, V_8, V_9, V_{10}, V_{19}, V_{20}, V_{22}, and V_{23}. Fig. 5 illustrates the instant of selecting the set of nearest voltage vectors to the optimal voltage vector V_{21}. Here, the voltage vectors V_1 and V_2 represent small vectors, V_7, V_8, V_9, and V_{10} represent medium vectors, and V_{19}, V_{20}, V_{22}, and V_{23} represent large vectors. Null vector (V_0) is always engaged with the active vectors $(V_1–V_{36})$ for reduction of torque and

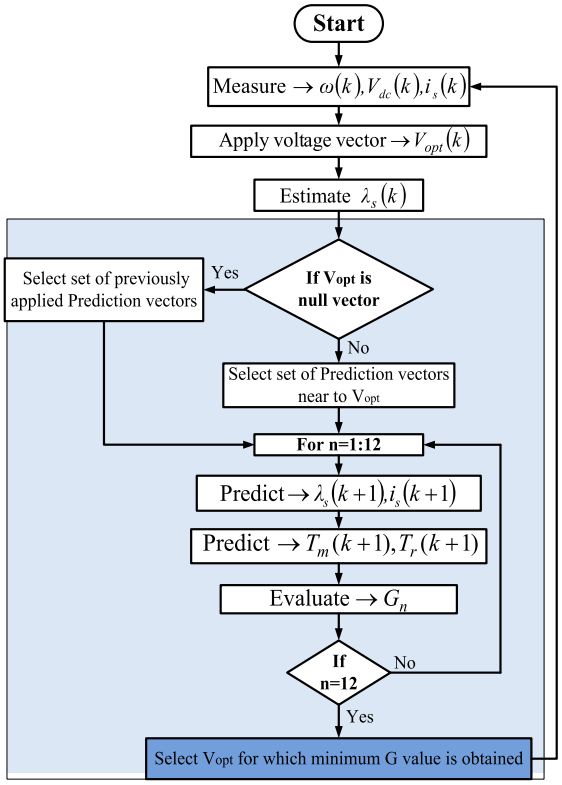

Fig. 6. Proposed PTC flow graph.

flux ripples. These voltage vectors (see Fig. 5) along with V_{21} are made available for the next sample interval as a set of prediction voltage vectors for the cost function evaluation. Consider one more case, where the null voltage vector V_0 is selected as optimal, in this situation the previous set of prediction voltage vectors are considered for the present cost function evaluation.

Thus in each sample interval, cost function is evaluated for only 12 prediction voltage vectors, instead of evaluating for all the 37 voltage vectors. This proposed feature permits reduction in computational burden of control process and also it adds switching frequency limitation as the next selecting optimal voltage vector is nearer to the previously selected optimal voltage vector. The overall control steps involved in the proposed PTC are exhibited in Fig. 6 and are discussed as follows.

Step 1: Measure combined dc link voltage ($V_{\rm dc}$), stator current space vector (i_s), and motor speed (ω_r).

Step 2: Estimate present stator flux [$\lambda_s(k)$] with the information of previously applied optimal voltage vector [$V_s(k-1)$], stator flux and current.

Step 3: Follow the nearest voltage vector strategy [set of voltage vectors nearer to the $V_s(k-1)$] and limit the number of prediction voltage vectors for the prediction in next sample interval.

Step 4: With the help of limited prediction voltage vectors, Predict stator flux [$\lambda_s(k+1)$] and current [$i_s(k+1)$], which further provides active torque [$T_m(k+1)$] and reactive torque [$T_r(k+1)$] predictions.

Step 5: Evaluate the modified cost function G_n (24), with the limited predicted values of active torque and reactive torque (obtained from the limited prediction voltage vectors).

Step 6: Select the optimal voltage vector for the next sample interval providing minimum cost function value and apply its corresponding switching states to the dual inverter.

Thus, a simplified PTC of OEWIM drive, eliminating weighting factor requirement in cost function and limiting prediction voltage vectors without any additional computational burden, is achieved.

TABLE II
OEWIM SPECIFICATIONS

Motor Parameter	Quantity
Poles (P)	4
Rated speed	1440 RPM
Rated Power	3.7 kW
Rated Torque	24.5 Nm
Inertia (J)	0.031 kg-m^2
Stator Resistance (R_s)	1.8 Ω
Rotor Resistance (R_r)	0.8 Ω
Stator Inductance (L_s)	0.54 H
Rotor Inductance (L_r)	0.54 H
Mutual Inductance (L_m)	0.512 H

V. RESULTS AND DISCUSSION

The proposed PTC for OEWIM drive is verified by performing MATLAB simulation and real-time experimentation. The machine parameters of real-time test setup are given in Table II. The obtained results of the proposed PTC are compared with the classical PTC scheme. For this, classical PTC is executed with the cost function given in (23) and evaluated for all the 37 prediction voltage vectors of dual inverter in each sample period. In (23), for flux weighting factor (W_f) determination, heuristic procedure is followed and the value of it is considered as 75.

A. Simulation Results

The proposed PTC for OEWIM drive is implemented in MATLAB/Simulink software. The dual-inverter fed OEWIM drive mathematical modeling is performed in Simulink by considering (1)–(12) and real-time parameter values (as listed in Table II) are assigned to it. The combined dc link voltage ($V_{\rm dc}$) of dual inverter is taken as 500 V, i.e., VSI-1 dc link voltage is set to 333.33 V and for VSI-2, it is set to 166.67 V.

To assess the effectiveness of the proposed PTC over classical scheme, MATLAB simulations are executed at different operating conditions of motor at no load. The obtained simulation results of both proposed and classical PTC are shown in Fig. 7. Till the simulation time of 2 s, motor reference speed is set to +150 rad/s (electrical). During this time interval, motor exhibit steady-state forward speed, torque, flux, and current response. At the simulation time of 2 s, step change in motor

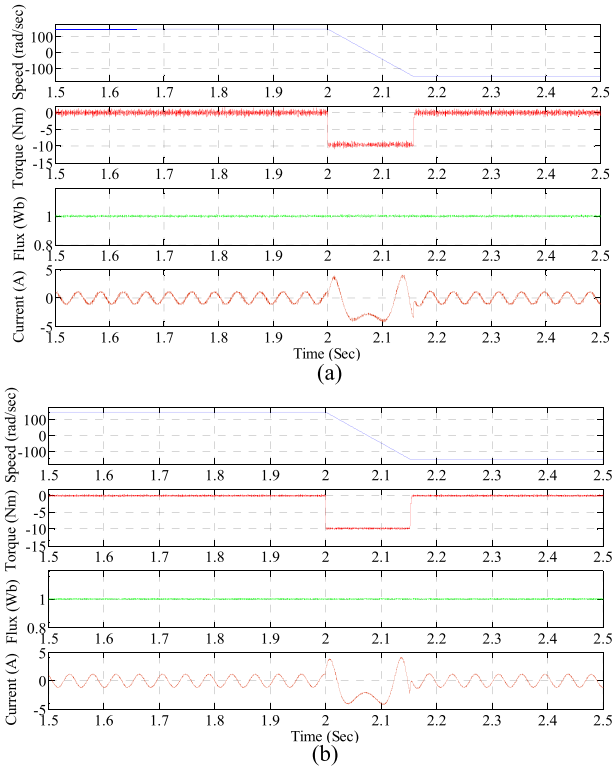

Fig. 7. Simulated speed, torque, flux, and current response of OEWIM drive. (a) Classical PTC. (b) Proposed PTC.

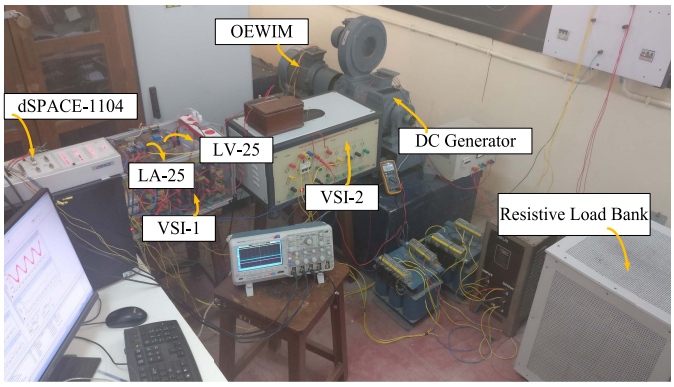

Fig. 8. OEWIM drive test setup.

reference speed is given from +150 to −150 rad/s. During this instant, motor speed, torque, and current dynamic response are observed. After the time instant of 2.15 s, motor speed settles at −150 rad/s, indicating reverse motoring operation. The steady-state reverse speed, torque, flux, and current response are observed.

From Fig. 7(a) and (b), it is observed that both classical and proposed PTCs of OEWIM performed similar dynamic characteristics. Improved steady-state torque, flux, and current response are achieved for the proposed PTC of OEWIM in Fig. 7(b). Thus, it is verified that better steady-state response of OEWIM drive is achieved by implementing the proposed PTC scheme than the classical PTC.

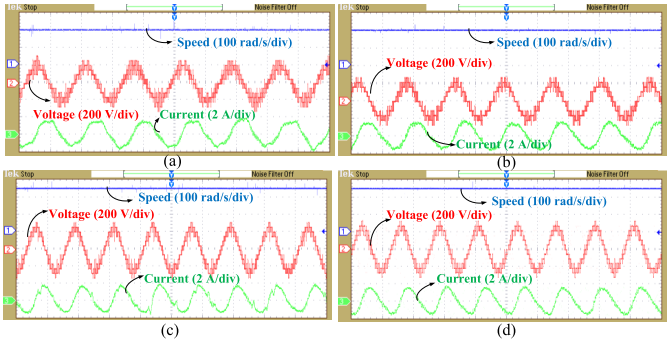

Fig. 9. Experimental steady-state motor speed, voltage, and current response. (a) With classical PTC and (b) proposed PTC of OEWIM running at 200 rad/s. (c) With classical PTC and (d) proposed PTC of OEWIM running at 250 rad/s (x-axis timescale—20 ms/div).

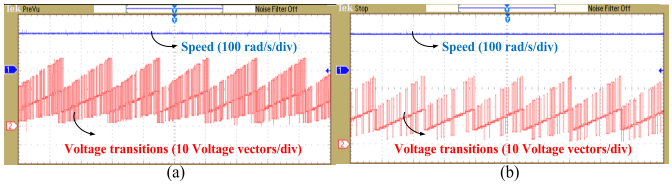

Fig. 10. Dual-inverter voltage-state transitions at motor speed of 200 rad/s. (a) Classical PTC and (b) proposed PTC (x-axis timescale—20 ms/div).

B. Experimental Results

The real-time validation of the proposed PTC is exhibited by performing experimentation on 3.7-kW OEWIM drive. The OEWIM is coupled with dc generator, in order to apply load torque on motor by loading dc generator with a resistive load. Fig. 8 depicts experimental test setup of OEWIM drive. For real-time execution, MATLAB software is interfaced with dSPACE RTI 1104 controller. The inputs to the PTC algorithm are combined dc link voltage ($V_{\rm dc}$), motor speed (ω_r), and current (i_s). Motor speed is measured with encoder and connected to dSPACE incremental encoder. DC link voltage and motor phase currents are sensed from the sensors LV-25 and LA-25, respectively. These sensed signals are given to analog to digital converter-Bayonet Neill–Concelman connectors of dSPACE control board. The optimal switching states of dual inverter achieved from the PTC algorithm are given to the dSPACE Master bit I/O pins and thereby interfacing with the dual-inverter switches. The conducted experimentation results of both conventional and proposed PTCs for various operating conditions of motor are shown in Figs. (9)–(17).The speed and flux PI regulator gains are tuned empirically. In fact the tuning of PI regulators is easier when compared to the weighting factor tuning [38].

During no-load condition, motor is operated at the reference speeds 200 and 250 rad/s (electrical). Its steady-state speed, phase voltage, and current response are shown in Fig. 9. Fig. 9(a) and (c) are the motor response at reference speeds 200 and 250 rad/s when classical PTC technique is used for motor control. At the same speeds, Fig. 9(b) and (d) are the motor response obtained for the proposed PTC scheme. The improved voltage and current response is achieved in the proposed PTC scheme than the classical PTC. When the motor

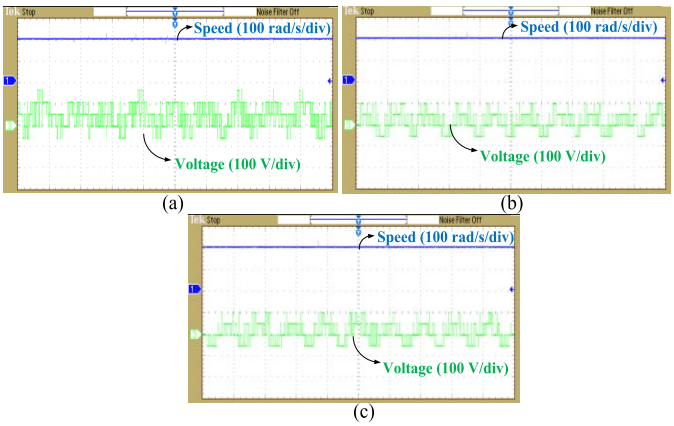

Fig. 11. OEWIM drive CMV response at a reference speed of 200 rad/s. (a) Conventional PTC, (b) PTC [33], and (c) proposed PTC (x-axis timescale—10 ms/div).

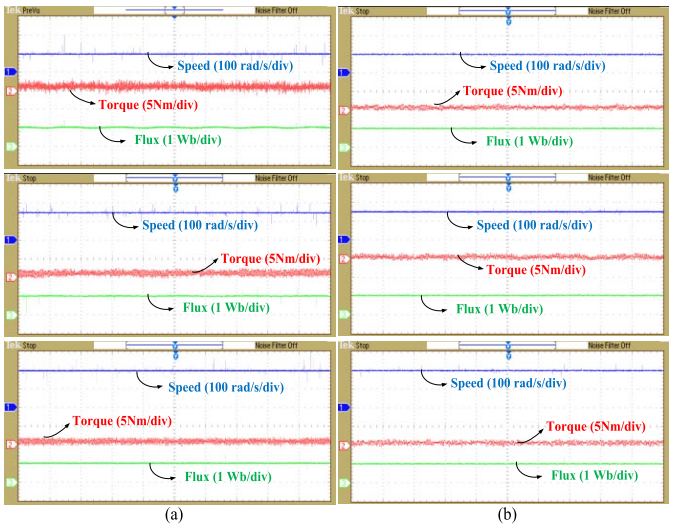

Fig. 12. Experimental steady-state motor speed, torque, and flux response. (a) With classical PTC and (b) proposed PTC of OEWIM running at 100, 150, and 200 rad/s (x-axis timescale—20 ms/div).

reference speed is set to 200 rad/s, the response of motor speed and dual-inverter switching transitions are shown in Fig. 10. Fig. 10(a) and (b) shows the experimental response for the classical and proposed PTC schemes, respectively. With the help of nearest voltage vector selection strategy in the proposed PTC, the nearest limited voltage vectors set to the optimal one (which is selected in previous state) is made available for the present cost function evaluation. Thus, the optimal voltage vector selection for the next sample interval is mostly nearer to the previous one. Thereby, reducing switching state transitions. In Fig. 10(b), less dual-inverter switching state transitions are observed in the proposed PTC compared to classical PTC scheme. Number of switching state transitions in a fixed time period decides the dual-inverter average switching frequency. Thus, the average switching frequency reduction is achieved in the proposed PTC scheme.

In Fig. 11, the effect of CMV is observed. The reduction in CMV is observed for the proposed PTC as the proposed PTC

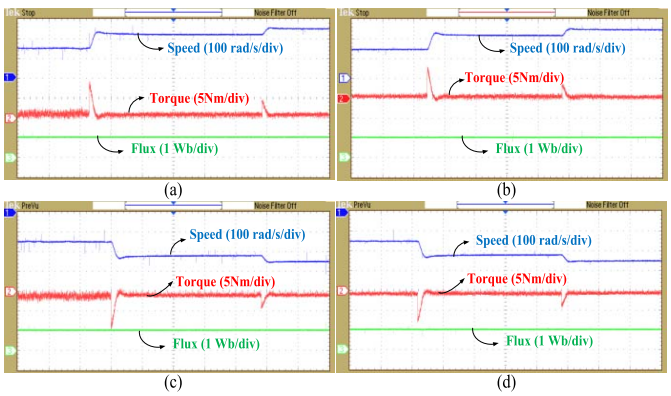

Fig. 13. Experimental dynamic response of motor speed, torque, and flux. (a) With classical PTC and (b) proposed PTC of OEWIM running at step changes in forward speed from 150 to 220 rad/s and finally 250 rad/s. (c) With classical PTC and (d) proposed PTC of OEWIM running at step changes in reverse speed from −150 to −220 rad/s and finally −250 rad/s (x-axis timescale—2 s/div).

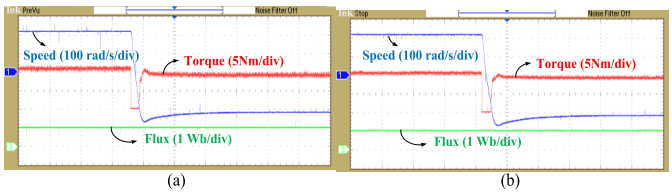

Fig. 14. Experimental dynamic response of OEWIM drive from forward (+220 rad/s) to reverse motoring (−220 rad/s). (a) With classical PTC and (b) proposed PTC (x-axis timescale—1 s/div).

of OEWIM drive operates at lower switching frequency. The observed CMV rms values at motor speed of 200 rad/s for the conventional, PTC [33] and the proposed PTC are 67.7, 51.2, and 50.1 V, respectively. At the reference speed of 100, 150, and 200 rad/s, the steady-state motor speed, torque, and flux response are shown in Fig. 12. Fig. 12(a) represents the experimental response obtained for classical PTC of OEWIM running at 100, 150, and 200 rad/s. At the same speeds, Fig. 12(b) represents the motor response obtained for the proposed PTC scheme, where the optimal torque and flux response are observed. Thus, the reduction in motor steady-state torque and flux ripple are achieved in the proposed PTC scheme for OEWIM.

In Fig. 13, dynamic response of OEWIM is observed during forward and reverse motoring operations. For dynamic analysis of motor, dSPACE Control Desk software is used to trigger the reference speeds online. During the operation of motor at speed of 150 rad/s, step change in reference speed is given from +150 to +220 rad/s and finally +250 rad/s. The motor exhibited dynamic responses of speed, torque, and flux for both classical and proposed PTCs that are shown in Fig. 13(a) and (b), respectively.

During reverse motoring operation, for the same step changes in reference speeds, i.e., −150 to −220 rad/s and finally −250 rad/s, the exhibited dynamic responses of motor for the both classical and proposed PTCs are shown in Fig. 13(c) and (d), respectively. In Fig. 14, forward to

TABLE III

COMPARISON OF TORQUE RIPPLE, FLUX RIPPLE, AND AVERAGE SWITCHING FREQUENCY ACHIEVED IN THE PROPOSED PTC OF OEWIM DRIVE AND EXISTING ONES IN THE LITERATURE

Motor speed (rad/sec)	Torque ripple (Nm)			Flux ripple (Wb)			Switching frequency (Hz)		
	Classical PTC	In [33] PTC with OEWIM drive	Proposed PTC	Classical PTC	In [33] PTC with OEWIM drive	Proposed PTC	Classical PTC	In [33] PTC with OEWIM drive	Proposed PTC
100	1.77	1.48	1.21	0.033	0.03	0.023	4018	2658	2528
200	1.401	1.24	1.16	0.022	0.02	0.015	4724	3226	3104
250	1.09	1.01	0.804	0.018	0.011	0.008	4458	2984	2962

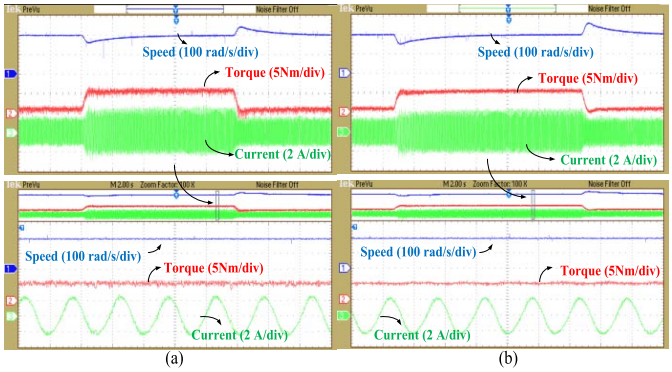

Fig. 15. Experimental dynamic response of OEWIM drive with the load disturbance operating at a speed of 200 rad/s. (a) With classical PTC and (b) proposed PTC (x-axis timescale—2 s/div and zoomed-in view x-axis timescale—20 ms/div).

reverse motoring characteristics are shown. While motor is operating in forward direction at a speed of +220 rad/s, step change of −220 rad/s is triggered. During this operation, the motor speed, torque, and flux response for both classical and proposed PTCs are shown in Fig. 14(a) and (b), respectively.

In Fig. 15, dynamic response of OEWIM with the load disturbance is observed. During no load, while motor is operating at the speed of 200 rad/s, load torque of 5 N·m is applied and removed after certain time. The exhibited motor dynamic speed, torque, and current responses for both classical and proposed PTC schemes are shown in Fig. 15(a) and (b), respectively.

From these experimental results, it is observed that both classical and proposed PTC schemes exhibited almost similar dynamic characteristics during step change in reference speed and load torque disturbance. The prominence of the proposed PTC is observed during the steady-state operation of motor exhibiting low torque and flux ripple at different operating speeds compared to the classical PTC scheme. Thus, the weighting factor elimination in modified cost function of the proposed PTC results in better control response of motor drive, i.e., improved torque and flux regulation. Furthermore, the nearest voltage vector selection scheme facilitates the benefits of reduced computation time and switching frequency reduction without affecting the motor drive response achieved when all the voltage vectors are involved in the evaluation of modified cost function. The proposed PTC of OEWIM drive is tested at rated speed of 1440 RPM (301 rad/s-electrical)

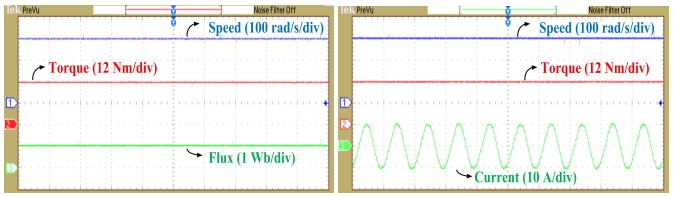

Fig. 16. OEWIM drive response for the proposed PTC at a speed of 301 rad/s and a load torque of 24.5 N·m (x-axis timescale—20 ms/div).

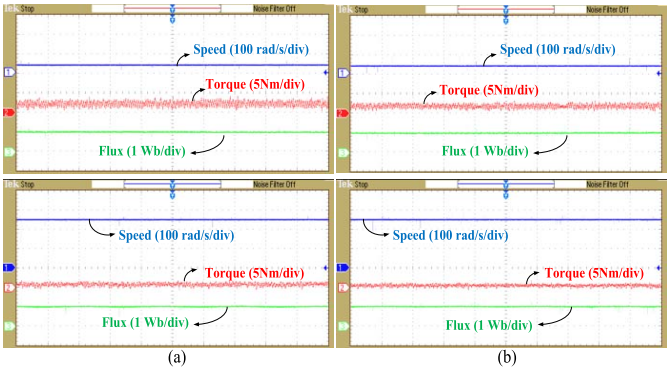

Fig. 17. OEWIM drive speed, torque, and flux response. (a) PTC [33] and (b) proposed PTC (x-axis timescale—20 ms/div).

and full load torque condition. The experimental results of OEWIM drive response are shown in Fig. 16.

Comparison of torque, flux ripple, and average switching frequency at various operating speeds among the classical PTC, PTC [33] performed with OEWIM drive, and the proposed PTC of OEWIM is listed in Table III. The torque and flux ripples are calculated by considering the sum of the difference between the measured and reference over 125 000 samples. From these results, it is validated that the proposed PTC exhibits better steady-state torque and flux response. The concept of PTC in [33] is implemented for OEWIM drive control, where the flux weighting factor is eliminated. To limit the switching frequency in PTC [33], switching frequency control objective is added in cost function as given in [33, eq. (18)], which again demands switching frequency weighting factor assignment to it (without considering third term which is specific to NPC scheme). The selection of proper switching frequency weighting factor value in cost function, decides the optimal voltage vector selection.

TABLE IV
COMPARISON OF AVERAGE COMPUTATION TIMES ACHIEVED IN THE PROPOSED PTC OF OEWIM DRIVE AND EXISTING ONES IN THE LITERATURE

Implementation method	Overall Computational time
In Classical PTC	60 μsec
In [33] PTC with OEWIM drive	46.8 μsec
Proposed PTC	34.2 μsec

The comparative results of speed, torque, and flux obtained for PTC [33] and the proposed PTC are shown in Fig. 17.

The top results in Fig. 17 indicate low-speed operation of 40 rad/s with very light-load condition and bottom results indicate high-speed operation of 250 rad/s at no-load condition. For limiting number of prediction voltage vectors, stator flux error strategy is followed for PTC [33] of OEWIM drive. It demands 20 prediction voltage vectors in each sample interval, whereas for the proposed PTC only 12 prediction voltage vectors are required without any additional computational burden in control process. The total computation time for the proposed PTC of OEWIM drive in comparison with classical PTC and [33] is listed in Table IV.

Thus from the entire results, it is evident that the proposed PTC of OEWIM drive facilitate simple control structure, optimal torque and flux response, and switching frequency reduction with low computational burden when compared to the classical and PTC [33] implemented with OEWIM drive.

VI. CONCLUSION

In this paper, an improved predictive torque and flux control scheme for OEWIM drive with four-level inversion has been proposed which is independent of flux weighting factor. To achieve this, flux control objective is replaced by an equivalent reactive torque control. Furthermore, number of prediction voltage vectors selection in each sample interval is reduced to 12 from 37 which are used in the case of classical PTC. The reduction in number of prediction voltage vectors in each sample interval is achieved by nearest voltage vector selection strategy, which allows switching frequency reduction and thereby decrease in CMV. Thus providing overall simple control without any additional complex calculations and alleviating the problems faced by classical PTC of OEWIM drive.

The reliability of the proposed PTC is verified by conducting simulation and experimental assessment on dual-inverter fed OEWIM drive. From the conducted tests, it is evident that the proposed PTC offers improved steady-state torque and flux response. Lower torque, flux ripple, and average switching frequency reduction are observed for different operating conditions of OEWIM drive when compared to the classical PTC. Furthermore, the proposed PTC offers lower computation time when compared to the other PTC schemes of OEWIM drive. In the future, the proposed PTC scheme can be extended to improve its robustness toward the model parameter variations. Therefore, it is very clear that the proposed PTC gains all these benefits and this simple improved control technique is applicable for OEWIM drive control.

REFERENCES

[1] S. Kouro *et al.*, "Recent advances and industrial applications of multilevel converters," *IEEE Trans. Ind. Electron.*, vol. 57, no. 8, pp. 2553–2580, Aug. 2010.

[2] K. K. Gupta, A. Ranjan, P. Bhatnagar, L. K. Sahu, and S. Jain, "Multilevel inverter topologies with reduced device count: A review," *IEEE Trans. Power Electron.*, vol. 31, no. 1, pp. 135–151, Jan. 2016.

[3] N. Mittal, B. Singh, S. P. Singh, R. Dixit, and D. Kumar, "Multilevel inverters: A literature survey on topologies and control strategies," in *Proc. 2nd Int. Conf. Power, Control Embedded Syst.*, Allahabad, India, 2012, pp. 1–11.

[4] J. Rodríguez, J.-S. Lai, and F. Z. Peng, "Multilevel inverters: A survey of topologies, controls, and applications," *IEEE Trans. Ind. Electron.*, vol. 49, no. 4, pp. 724–738, Aug. 2002.

[5] S. Lakhimsetty, N. Surulivel, and V. T. Somasekhar, "Improvised SVPWM strategies for an enhanced performance for a four-level open-end winding induction motor drive," *IEEE Trans. Ind. Electron.*, vol. 64, no. 4, pp. 2750–2759, Apr. 2017.

[6] F. Blaschke, "The principle of field orientation as applied to the new transvector closed-loop system for rotating-field machines," *Siemens Rev.*, vol. 34, no. 4, pp. 217–220, 1972.

[7] S. Sathikumar and J. Vithayathil, "Digital simulation of field-oriented control of induction motor," *IEEE Trans. Ind. Electron.*, vol. IE-31, no. 2, pp. 141–148, May 1984.

[8] I. Takahashi and T. Noguchi, "A new quick-response and high-efficiency control strategy of an induction motor," *IEEE Trans. Ind. Appl.*, vol. IA-22, no. 5, pp. 820–827, Sep. 1986.

[9] K.-B. Lee, J.-H. Song, I. Choy, and J.-Y. Yoo, "Torque ripple reduction in DTC of induction motor driven by three-level inverter with low switching frequency," *IEEE Trans. Power Electron.*, vol. 17, no. 2, pp. 255–264, Mar. 2002.

[10] K. K. Shyu, J. K. Lin, V. T. Pham, M. J. Yang, and T. W. Wang, "Global minimum torque ripple design for direct torque control of induction motor drives," *IEEE Trans. Ind. Electron.*, vol. 57, no. 9, pp. 3148–3156, Sep. 2010.

[11] R. Ramchand, K. Gopakumar, C. Patel, K. Sivakumar, A. Das, and H. Abu-Rub, "Online computation of hysteresis boundary for constant switching frequency current-error space-vector-based hysteresis controller for VSI-fed IM drives," *IEEE Trans. Power Electron.*, vol. 27, no. 3, pp. 1521–1529, Mar. 2012.

[12] V. T. Kumar and S. S. Rao, "Reduction of torque ripple in direct torque control of induction motor using constant switching frequency operation," in *Proc. 7th Medit. Conf. Exhibit. Power Generat., Transmiss., Distrib. Energy Convers. (MedPower)*, Agia Napa, Cyprus, Nov. 2010, pp. 1–6.

[13] K. V. P. Kumar and T. V. Kumar, "Experimental implementation of direct torque control of open end winding induction motor," in *Proc. IEEE Region 10 Conf. (TENCON)*, Singapore, Nov. 2016, pp. 3318–3323.

[14] A. Linder and R. Kennel, "Model predictive control for electrical drives," in *Proc. IEEE 36th Power Electron. Spec. Conf. (PESC)*, Jun. 2005, pp. 1793–1799.

[15] F. Wang, Z. Zhang, R. Kennel, and J. Rodríguez, "Model predictive torque control with an extended prediction horizon for electrical drive systems," *Int. J. Control*, vol. 88, no. 7, pp. 1379–1388, 2015.

[16] V. Yaramasu, M. Rivera, M. Narimani, B. Wu, and J. Rodríguez, "Finite state model-based predictive current control with two-step horizon for four-leg NPC converters," *J. Power Electron.*, vol. 14, no. 6, pp. 1178–1188, 2014.

[17] D. Zhou, J. Zhao, and Y. Li, "Model-predictive control scheme of five-leg AC–DC–AC converter-fed induction motor drive," *IEEE Trans. Ind. Electron.*, vol. 63, no. 7, pp. 4517–4526, Jul. 2016.

[18] D. Zhou, J. Zhao, and Y. Liu, "Predictive torque control scheme for three-phase four-switch inverter-fed induction motor drives with DC-link voltages offset suppression," *IEEE Trans. Power Electron.*, vol. 30, no. 6, pp. 3309–3318, Jun. 2015.

[19] J. Rodríguez and P. Cortes, "Predictive control of induction machines," in *Predictive Control of Power Converters and Electrical Drives*. New York, NY, USA: Wiley, 2012, pp. 115–132.

[20] P. Cortes *et al.*, "Guidelines for weighting factors design in model predictive control of power converters and drives," in *Proc. IEEE Int. Conf. Ind. Technol. (ICIT)*, Feb. 2009, pp. 1–7.

[21] P. Zanchetta, "Heuristic multi-objective optimization for cost function weights selection in finite states model predictive control," in *Proc. Workshop Predictive Control Elect. Drives Power Electron.*, Oct. 2011, pp. 70–75.

[22] M. Uddin, S. Mekhilef, M. Mubin, and M. Rivera "Model predictive torque ripple reduction with weighting factor optimization fed by an indirect matrix converter," *Electr. Power Compon. Syst.*, vol. 42, no. 10, pp. 1059–1069, 2014.
[23] R. Vargas, U. Ammann, B. Hudoffsky, J. Rodríguez, and P. Wheeler, "Predictive torque control of an induction machine fed by a matrix converter with reactive input power control," *IEEE Trans. Power Electron.*, vol. 25, no. 6, pp. 1426–1438, Jun. 2010.
[24] D. Zhou, J. Zhao, and Y. Liu, "Online tuning of weighting factors based on sugeno fuzzy method in predictive torque control of four-switch three-phase inverter-fed IM," in *Proc. Int. Symp. Power Electron., Elect. Drives, Autom. Motion*, 2016, pp. 734–739.
[25] C. A. Rojas, S. Kouro, M. Perez, and F. Villarroel, "Multiobjective fuzzy predictive torque control of an induction machine fed by a 3L-NPC inverter," in *Proc. IEEE Int. Symp. Predictive Control Elect. Drives Power Electron.*, Oct. 2015, pp. 21–26.
[26] M. B. Shadmand, R. S. Balog, and H. A. Rub, "Auto-tuning the cost function weight factors in a model predictive controller for a matrix converter VAR compensator," in *Proc. IEEE Energy Convers. Congr. Expo. (ECCE)*, Montreal, QC, Canada, Sep. 2015, pp. 3807–3814.
[27] C. A. Rojas, J. Rodríguez, F. Villarroel, J. R. Espinoza, C. A. Silva, and M. Trincado, "Predictive torque and flux control without weighting factors," *IEEE Trans. Ind. Electron.*, vol. 60, no. 2, pp. 681–690, Feb. 2013.
[28] K. V. P. Kumar and T. V. Kumar, "Predictive torque control of open-end winding induction motor drive fed with multilevel inversion using two two-level inverters," *IET Electr. Power Appl.*, vol. 12, no. 1, pp. 54–62, 2017, doi: 10.1049/iet-epa.2017.0209.
[29] V. P. Muddineni, A. K. Bonala, and S. R. Sandepudi, "Enhanced weighting factor selection for predictive torque control of induction motor drive based on VIKOR method," *IET Electr. Power Appl.*, vol. 10, no. 9, pp. 877–888, 2016.
[30] V. P. Muddineni, S. R. Sandepudi, and A. K. Bonala, "Finite control set predictive torque control for induction motor drive with simplified weighting factor selection using TOPSIS method," *IET Electr. Power Appl.*, vol. 11, no. 5, pp. 749–760, 2017.
[31] B. Zhu, K. Rajashekara, and H. Kubo, "Predictive torque control with zero-sequence current suppression for open-end winding induction machine," in *Proc. IEEE Ind. Appl. Soc. Annu. Meeting*, Addison, TX, USA, Oct. 2015, pp. 1–7.
[32] M. Habibullah, D. D.-C. Lu, D. Xiao, and M. F. Rahman, "A simplified finite-state predictive direct torque control for induction motor drive," *IEEE Trans. Ind. Electron.*, vol. 63, no. 6, pp. 3964–3975, Jun. 2016.
[33] M. Habibullah, D. D.-C. Lu, D. Xiao, J. E. Fletcher, and M. F. Rahman, "Low complexity predictive torque control strategies for a three-level inverter driven induction motor," *IET Electr. Power Appl.*, vol. 11, no. 5, pp. 776–783, 2017.
[34] Y. Zhang and H. Yang, "Two-vector-based model predictive torque control without weighting factors for induction motor drives," *IEEE Trans. Power Electron.*, vol. 31, no. 2, pp. 1381–1390, Feb. 2016.
[35] K. V. P. Kumar, K. M. R. Eswar, and T. V. Kumar, "Hardware implementation of Predictive Torque Controlled Open-end winding induction motor drive with self-tuning algorithm," *Cogent Eng.*, vol. 4, no. 1, p. 1388206, 2017.
[36] J. Guzinski, "Common-mode voltage and bearing currents in PWM inverters: Causes, effects and prevention," in *Power Electronics for Renewable Energy Systems, Transportation and Industrial Applications*. Hoboken, NJ, USA: Wiley, 2014, pp. 664–694.
[37] P. Vas, *Sensorless Vector and Direct Torque Control*. London, U.K.: Oxford Univ. Press, 1998.
[38] J. Rodríguez *et al.*, "State of the art of finite control set model predictive control in power electronics," *IEEE Trans. Ind. Informat.*, vol. 9, no. 2, pp. 1003–1016, May 2013.

Kodumur Meesala Ravi Eswar was born in Kurnool, India, in 1993. He received the B.Tech. degree from Jawaharlal Nehru Technological University, Ananthapur, India, in 2014, and the M.Tech. degree from the Vellore Institute of Technology, Vellore, India, in 2016. He is currently pursuing the Ph.D. degree with the Department of Electrical Engineering, National Institute of Technology, Warangal, India.

His current research interests include electric motor drive control, power electronics, and power converter circuits.

Kunisetti Venkata Praveen Kumar was born in Guntur, India, in 1990. He received the B.Tech. and M.Tech. degrees from Jawaharlal Nehru Technological University, Kakinada, India, in 2011 and 2014, respectively. He is currently pursuing the Ph.D. degree with the Department of Electrical Engineering, National Institute of Technology, Warangal, India.

His current research interests include electric motor drive control, power electronics, and power converter circuits.

Thippiripati Vinay Kumar (M'16) was born in Kadapa, India, in 1984. He received the B.Tech. and M.Tech. degrees from Jawaharlal Nehru Technological University, Hyderabad, India, in 2005 and 2008, respectively, and the Ph.D. degree from the National Institute of Technology, Warangal, India, in 2015.

In 2013, he joined the National Institute of Technology, as an Assistant Professor. His current research interests include power electronics and drives, direct torque control, predictive torque control, open-end winding induction motor drives, multilevel inverters, hybrid electric vehicles, and renewable energy interfacing.